



### **Science Arts & Métiers (SAM)**

is an open access repository that collects the work of Arts et Métiers Institute of Technology researchers and makes it freely available over the web where possible.

This is an author-deposited version published in: <https://sam.ensam.eu>  
Handle ID: <http://hdl.handle.net/10985/23585>

#### **To cite this version :**

Steven ARAUJO, Chloé SAINLAUD, Nicolas DELPOUVE, Emmanuel RICHAUD, Laurent DELBREILH, Eric DARGENT - Segmental Relaxation Dynamics in Amorphous Polylactide Exposed to UV Light - Macromolecular Chemistry and Physics, - Vol. 223, n°16, p.2200085 ( from 1 to 8) - 2022

Any correspondence concerning this service should be sent to the repository

Administrator : [scienceouverte@ensam.eu](mailto:scienceouverte@ensam.eu)



# Segmental Relaxation Dynamics in Amorphous Polylactide Exposed to UV Light

Steven Araujo, Chloé Sainlaud, Nicolas Delpouve,\* Emmanuel Richaud, Laurent Delbreilh, and Eric Dargent

The degradation of polylactide (PLA) under UV exposure is investigated in terms of cooperativity and kinetic fragility at the glass transition. In the first part, possibly coexisting degradation mechanisms are evoked from the interpretation of the infrared spectroscopy analyses. Furthermore, the reduction of PLA chain length, owing to photolytic scissions predominant over local crosslinks, is assessed from chromatography, and confirmed by the shift of the glass transition temperature toward lower temperature. Modulated temperature thermogravimetric analysis (MT-TGA) also shows that the activation energy needed to initiate thermal degradation falls after UV exposure. In the second part, the impact of UV-induced degradation on the cooperative rearranging region (CRR) size and the kinetic fragility, respectively, calculated thanks to calorimetric and dielectric measurements, is discussed. Despite the assumed concomitance of several degradation mechanisms, it is observed that the glass transition, the kinetic fragility, and the CRR size decrease together with the exposure time. Moreover, it is found that the data align well on another trend depicting the change in the relaxation properties caused by plasticization of PLA. Thus, the variations of segmental relaxation properties caused by UV may be related to the increase of free volume linked to the damaging of the PLA structure.

## 1. Introduction

Polylactide (PLA) is a bio-based polymer, which exhibits interesting properties for packaging and biomedical purposes notably.<sup>[1,2]</sup> Its weaknesses, commonly mentioned in the literature, include its brittleness and its moderate barrier properties, limiting its industrial production.<sup>[3,4]</sup> On the other hand, the high amount of work dedicated to improve PLA properties in both

academic and industrial fields has recently led to consider its use for applications requiring long-term performance.<sup>[5]</sup> As a consequence, the concern about PLA stability is expected to grow. When knowledge about the amorphous phase, less stable than the crystalline one, is needed to better approach the macroscopic properties, the investigation of relaxation dynamics offers an interesting complement to the structural characterization. For example, by investigating glass transition dynamics in neat and plasticized PLA, we recently correlated the scale of the cooperative motions, i.e., the cooperative rearranging region (CRR) size, with the free volume, which plays a significant role in the diffusion processes.<sup>[6]</sup>

The CRR concept has been introduced by Adam and Gibbs.<sup>[7]</sup> A CRR is defined as the smallest subsystem in which the relaxation occurs independently from the neighboring subsystems. It is thus characterized by its own relaxation dynamics and its own thermodynamics variables. Although known since decades, the CRR concept has recently received a regain of

interest to link the relaxation dynamics with the molecular architecture.<sup>[8–12]</sup> Dhotel et al.<sup>[8]</sup> have evidenced that cooperative motions become predominant over local motions in self-assembled monolayers due to the organization of end groups into a relaxation canopy. Grigoros and Grigoros<sup>[9]</sup> reported that the cooperativity is influenced by the ratio between electrodonor and electroacceptor groups in statistical methacrylate copolymers. Nakanishi and Nozaki<sup>[10]</sup> proposed a hydrogen-bonding model supporting the increase of the CRR size with intermolecular interactions. Sasaki et al.<sup>[11]</sup> reported that the cooperativity decreases when the crosslinking density increases in bulk polystyrenes and poly(methyl methacrylate)s. Araujo et al.<sup>[12]</sup> reported that the breaking of interchain bonds by plasticization decreases the cooperativity in PLA. These results, among others, show that the CRR concept is a useful tool to get information on the polymer structure.

Data regarding the CRR size have been confronted with the kinetic fragility<sup>[6,12–17]</sup> depicting the temperature dependence of the relaxation time when approaching the glass transition from the supercooled liquid.<sup>[18]</sup> PLA exhibits a high kinetic fragility index,<sup>[13]</sup> about 150, thus ranking among the polymers, for which the increase of the relaxation time is very abrupt close to the glass

S. Araujo, C. Sainlaud, N. Delpouve, L. Delbreilh, E. Dargent  
UNIROUEN Normandie, Normandie Univ., INSA Rouen, CNRS, Groupe de Physique des Matériaux  
Rouen 76000, France  
E-mail: nicolas.delpouve1@univ-rouen.fr  
E. Richaud  
Laboratoire PIMM, Arts et Métiers Institute of Technology, CNRS, Cnam, HESAM Université, 151 Boulevard de l'Hopital  
Paris 75013, France

 The ORCID identification number(s) for the author(s) of this article can be found under <https://doi.org/10.1002/macp.202200085>

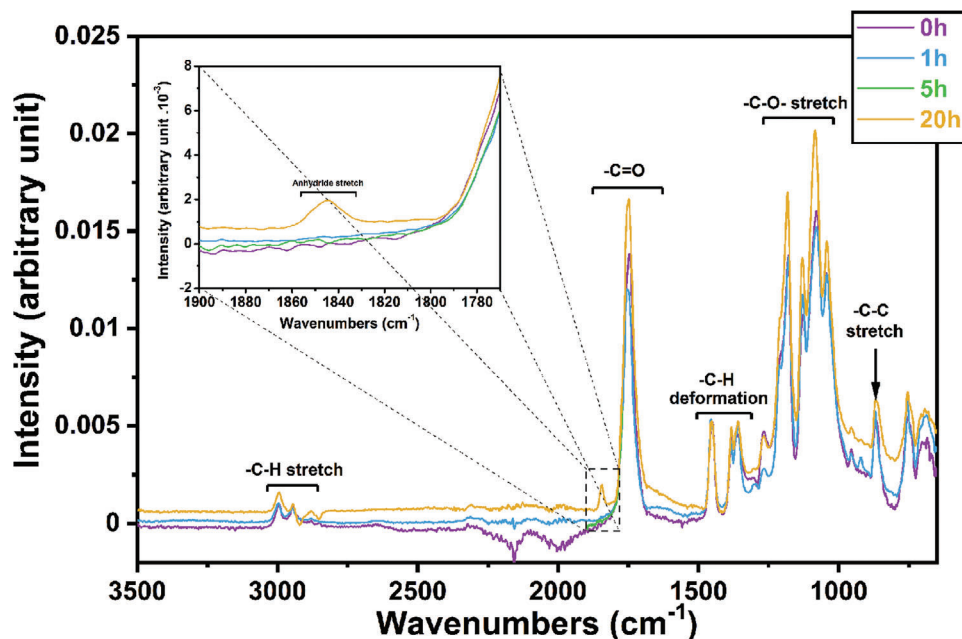


Figure 1. FTIR spectra recorded for PLA\_0h, PLA\_1h, PLA\_5h, and PLA\_20h.

transition. This value is notably high since more kinetically fragile polymers are often characterized by a stiff backbone.<sup>[19]</sup> It is assumed that the strongly cooperative character of PLA influences its kinetic fragility.<sup>[12]</sup> By the past, fragility and cooperativity have been tentatively connected with the chemical structure of polymers. Nevertheless, no systematic correlation between them is currently ascertained,<sup>[13–17]</sup> so plenty of questions are still under investigations.

Few studies deal with the impact of degradation on PLA segmental dynamics. Badia et al.<sup>[20]</sup> proposed from viscoelastic behavior investigations that the chain shortening induced by thermomechanical degradation is connected with an increase in the free volume. They evoked the possibility of a correlation with the cooperativity but did not perform this calculation. Besides, they investigated fragility from dielectric relaxation spectroscopy (DRS) in PLA submitted to repeated reprocessing cycles,<sup>[21]</sup> inducing a decrease of the molecular weight. However, the reported Arrhenius plots showed modest differences among samples, likely because reprocessing does not induce dramatic modifications of the macromolecular architecture, as can be deduced from the invariance of the glass transition temperature. Therefore, additional studies could benefit to the understanding of the relation between degradation-induced chain modifications and segmental dynamics.

In this study, we investigate how UV exposure impacts the segmental dynamics of PLA. The environmental conditions were intentionally severe enough to highlight the possible changes in relaxation parameters. Structural information was obtained from Fourier transform infrared (FT-IR) spectroscopy and gel permeation chromatography (GPC). Thermal stability of the UV-degraded PLA was addressed from modulated temperature thermogravimetric analysis (MT-TGA). Modulated temperature differential scanning calorimetry (MT-DSC) allowed determining the glass transition and calculating the CRR

size. Eventually, the kinetic fragility was obtained from DRS measurements.

## 2. Results and Discussion

### 2.1. Impact of UV Exposure on PLA Structural Features

The infrared signatures of PLA\_0h (no exposure) and UV-exposed PLA are shown in Figure 1. Basically, the main absorption band locations in PLA\_0h are<sup>[22–24]</sup> C–H stretch (2900–3000  $\text{cm}^{-1}$ ), C=O stretch (1700–1750  $\text{cm}^{-1}$ ), C–H deformation (1500–1350  $\text{cm}^{-1}$ ), C–O–C stretch (1300–1000  $\text{cm}^{-1}$ ), and C–C stretch (868  $\text{cm}^{-1}$ ). The whole spectra were normalized according to the reference peak located at 1453  $\text{cm}^{-1}$  of neat PLA,<sup>[22,23]</sup> corresponding to the  $\text{CH}_3$  asymmetric deformation.

For low exposure times (PLA\_1h and PLA\_5h), one can observe the appearance of a peak located around 900–950  $\text{cm}^{-1}$  (additional peak in the blue spectrum). According to Ikada,<sup>[25–27]</sup> this vibration band is one of the signatures characterizing the Norrish II mechanism of decomposition consecutive to chain scission. It is characterized by the formation of a C=C double bond during the step of termination, which occurs by dismutation. Moreover, low exposure times induce the decrease of the intensity of both C=O and C–O–C stretch vibration bands. Babanalbanti et al.<sup>[28]</sup> and Copinet et al.<sup>[29]</sup> listed the kind of radicals that could be formed during polylactide degradation. The first category regroups radicals associated with the breaking of C–C single bond of the main chain. The second category regroups radicals caused by the breaking of the ester function. The consequence of this breaking is the decrease of absorbance for C=O and C–O, as observed here. It is worth mentioning that the C=O stretch vibration band position can also reflect a decrease of the molecular weight as it indicates the proportion of free versus bound carbonyls.<sup>[30–32]</sup> Nevertheless, such investigation lies on

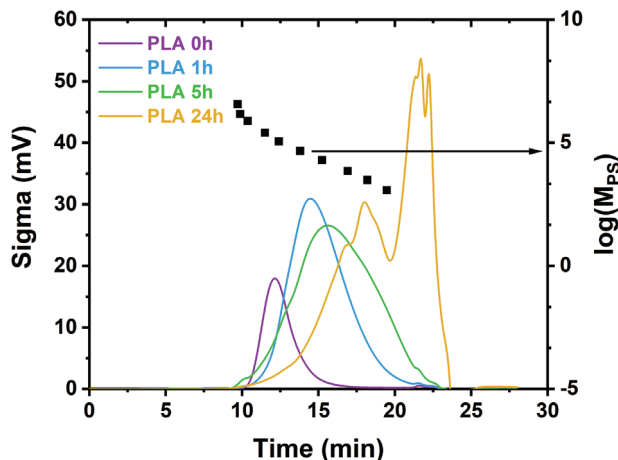


**Figure 2.** GPC chromatograms of PLA after various ageing times (left y-axis). (■) corresponds to the calibration with PS standards –y right axis).

the assumption that the samples only differ by their molecular weight, which is not guaranteed.

Indeed, for high exposure time (PLA\_20h), an additional peak shown in the inset is recorded at about  $1850\text{ cm}^{-1}$ . Contrary to the mechanisms evidenced for low exposure time, which are classically reported when working under nitrogen atmosphere, this additional vibration band is the consequence of the formation of anhydrides, which are subproducts of PLA decomposition mechanism under oxidative atmosphere, as described by Gardette et al.<sup>[24,27]</sup> The mechanism involves hydrogen abstraction on the polymeric backbone at the tertiary carbon in the  $\alpha$ -position of the ester function leading to the formation of macroradicals.<sup>[24]</sup> This suggests that the intervention of oxygen is not fully negated, with oxidative reactions evidenced for high exposure times. Accordingly, it can be seen for PLA\_24h that C=O and C–O–C stretch vibration bands' intensity is significantly increased compared to the other materials depicting an increased number of dipoles within the material. To summarize, concomitant photolysis and photo-oxidative degradation mechanisms are possible.

Chromatograms (Figure 2) have been converted into molar mass distribution values using the polystyrene (PS) calibration (allowing us to convert elution times into PS equivalent molar mass values). These were later converted into PLA molar mass value using the so-called calibration method according to which<sup>[33]</sup>  $[\eta]_{\text{PS}} \cdot M_{\text{PS}} = [\eta]_{\text{PLA}} \cdot M_{\text{PLA}}$  with intrinsic viscosity  $\eta$  being linked to molar mass  $M$  by the Mark–Houwink equation. The universal calibration method can be employed using the following coefficients  $[\eta] = 1.25 \times 10^{-2} \cdot M^{0.717}$  for PS and  $[\eta] = 5.49 \times 10^{-2} \cdot M^{0.639}$  for PLA valid in tetrahydrofuran (THF) at  $30\text{ }^{\circ}\text{C}$ .<sup>[34]</sup>

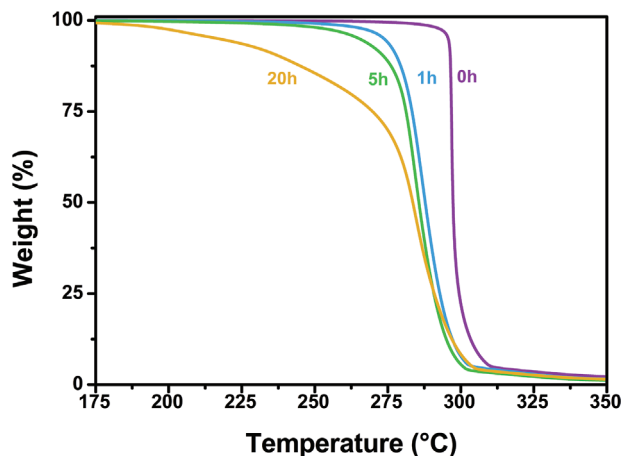


**Figure 3.** MT-TGA response versus temperature for PLA\_0h, PLA\_1h, PLA\_5h, and PLA\_20h.

PLA equivalent molar mass values were thus exploited using the relationships established by Saito,<sup>[35]</sup>  $1/M_n - 1/M_{n0} = s - x$  and  $1/M_w - 1/M_{w0} = s/2 - 2x$ , valid in the case of tetrafunctional crosslinking, thanks to which the concentration in random chain scissions  $s$  and crosslinking  $x$  can be estimated. The values are given in Table 1 and confirm that, in a first approach, chain scissions predominate over crosslinking. The calculation was not performed for PLA\_24h since the bimodal character of the chromatogram indicates various length distributions in consistence with our previous assumption of multiple concomitant degradation mechanisms. Furthermore, the molar masses have to be considered carefully due to the width of the size distribution.

The results regarding the thermal stability of neat and UV-exposed PLA investigated by MT-TGA are presented in Figure 3. The UV exposure impact on the thermal degradation process is followed by comparing the values  $T_x$  between samples where  $x$  is a given residual mass percentage. The thermal degradation of PLA\_0h occurs within a single step, with characteristic temperatures  $T_{90\%}$ ,  $T_{50\%}$ ,  $T_{10\%}$ , and  $T_{\text{max}}$ , which correspond to the maximum of the degradation rate, about 296, 297, 304 and 297  $^{\circ}\text{C}$  respectively (see Table 2). For PLA\_1h and PLA\_5h, the overall thermal degradation is shifted to lower temperatures. In the case of PLA\_20h, the first stages of degradation start at significantly lower temperatures in comparison with PLA\_0h, the mass loss being initiated at around 200  $^{\circ}\text{C}$  and  $T_{90\%}$  being equal to 238  $^{\circ}\text{C}$ . This shows that the UV exposure has a detrimental impact on the thermal stability.

MT-TGA has been previously used to calculate the activation energy related to decomposition,<sup>[36,37]</sup> with results consistent

**Table 1.** Number average ( $M_n$ ) and weight average ( $M_w$ ) molar mass values before and after ageing, polydispersity index (IP), and tentative exploitation to estimate concentration in chain scissions ( $s$ ) and crosslinking ( $x$ ).

	$M_n$ [g mol <sup>-1</sup> ]	$M_w$ [g mol <sup>-1</sup> ]	IP	$s - x$	$s/2 - 2x$	$s$	$x$
PLA_0h	60 000	120 000	2.0	0	0	0	0
PLA_1h	5300	30 000	5.8	$2 \times 10^{-4}$	$2 \times 10^{-5}$	$2 \times 10^{-4}$	$4 \times 10^{-5}$
PLA_5h	1700	28 000	16.5	$6 \times 10^{-4}$	$3 \times 10^{-5}$	$7 \times 10^{-4}$	$2 \times 10^{-4}$
PLA_24h	–	–	–	–	–	–	–

**Table 2.** MT-TGA results: characteristic degradation temperatures and the average activation energy calculated between 10% and 90% of mass loss for neat and UV-exposed PLAs.

	$T_{90\%}$ [°C]	$T_{50\%}$ [°C]	$T_{10\%}$ [°C]	$T_{max}$ [°C]	$E_{a,average}$ [kJ mol <sup>-1</sup> ]
PLA_0h	296	297	305	297	164
PLA_1h	278	288	298	287	154
PLA_5h	274	286	296	284	149
PLA_20h	238	284	297	284	147

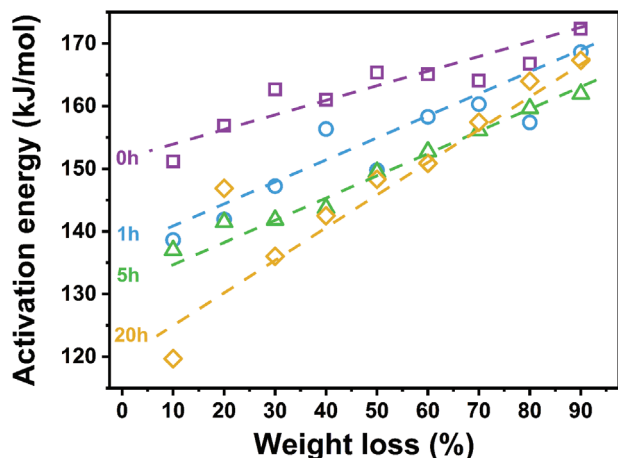


**Figure 4.** Activation energy variations within the degradation process for PLA\_0h, PLA\_1h, PLA\_5h, and PLA\_20h.

with those obtained by repeating scans at different rates from standard TGA.<sup>[38]</sup>

The activation energy  $E_a$  associated with the degradation of PLA\_0h slightly increases through the degradation process (Figure 4) and exhibits an average value  $E_{a,average} = 164$  kJ mol<sup>-1</sup>

within the interval  $T_{90\%} - T_{10\%}$ . By increasing the exposure time,  $E_{a,average}$  decreases ( $E_{a,average} = 147$  kJ mol<sup>-1</sup> for PLA\_20h). More evident, the activation energy strongly decreases during the early stages of degradation ( $E_a = 120$  kJ mol<sup>-1</sup> at  $T_{90\%}$  for PLA\_20h). These results are consistent with the FT-IR analysis, from which it can be deduced that UV exposure induces random chain scission into the macromolecular chains. According to McNeill and Leiper,<sup>[39]</sup> the main mechanism of thermal degradation occurs by a nonradical, backbiting ester interchange reaction involving the OH chain ends, proceeding with comparatively low energy of activation. Therefore, with the decrease of the molecular weight, the activation energy needed to initiate the degradation process is expected to be lower. One can also observe that the difference between samples in terms of  $E_a$  values becomes lesser with the thermolysis advancement, which may reveal that similar degradation subproducts are generated. On the other hand, at  $T_{10\%}$ ,  $E_a$  is higher in PLA\_20h than in PLA\_5h. Since FT-IR evidenced additional functions such as anhydrides in the structure of PLA\_20h in comparison to other UV-degraded PLAs, the possibility that stable species could result from thermolysis is not excluded either.

MT-DSC measurements were conducted on neat and irradiated PLA to investigate the impact of UV exposure on their molecular mobility (Figure 5). Subsequently, the discussion is focused on the glass transition region of PLA. As can be seen in Figure 5a, the UV exposure induces a shift of the glass transition signature toward lower temperature without significantly impacting the heat capacity step  $\Delta C_p$  (data given in Table 3). The dynamic glass transition temperature  $T_{aMT-DSC}$ , which corresponds to the maximum of the  $C''$  Gaussian fit (raw data given in Figure 5b), decreases from 333 to 317 K with the exposure time increasing from 0 to 24 h. Signori et al.<sup>[40]</sup> reported similar glass transition temperatures for PLAs exhibiting  $M_n$  equal to 120.0 and 71.2 kg mol<sup>-1</sup>, respectively. In consistence with GPC analyses, this shift of the glass transition should be the consequence of chain scissions. Similar observations were reported by Beslikas et al.<sup>[41]</sup> for hydrolyzed PLA.

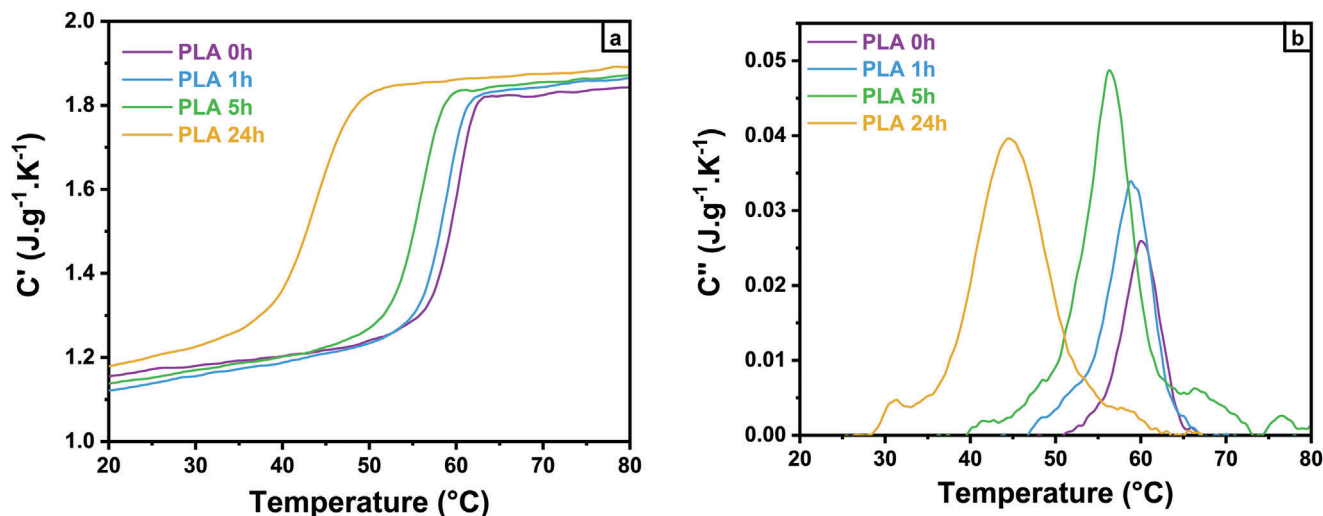


**Figure 5.** a) MT-DSC in-phase ( $C'$ ) component of the complex heat capacity and b) MT-DSC out of phase ( $C''$ ) component of the complex heat capacity for PLA\_0h, PLA\_1h, PLA\_5h, and PLA\_24h.

**Table 3.** Relaxation parameters obtained from MT-DSC and DRS for PLA\_0h, PLA\_1h, PLA\_5h, and PLA\_24h. Fragility values are given with an uncertainty of 10%.  $m_V$  and  $(m - m_V)$  are calculated for  $\alpha_T/\kappa = 1.5 \text{ MPa K}^{-1}$ .

	MT-DSC					DRS		
	$\Delta C_p [\text{J g}^{-1} \text{ K}^{-1}]$	$T_\alpha [\text{K}]$	$\delta T [\text{K}]$	$\xi_{T_\alpha}^3 [\text{nm}^3]$	$\xi_{T_\alpha} [\text{nm}]$	$T_\alpha (\tau = 100 \text{ s}) [\text{K}]$	$T_\alpha (\tau = 10 \text{ s}) [\text{K}]$	$m$
PLA_0h	$0.56 \pm 0.04$	$333 \pm 1$	$2.6 \pm 0.2$	$43.6 \pm 0.5$	$3.5 \pm 0.2$	$329 \pm 1$	$331 \pm 1$	158
PLA_1h	$0.57 \pm 0.04$	$332 \pm 1$	$3.4 \pm 0.2$	$25.7 \pm 0.5$	$3.0 \pm 0.2$	$326 \pm 1$	$328 \pm 1$	153
PLA_5h	$0.58 \pm 0.04$	$329 \pm 1$	$3.7 \pm 0.2$	$22.7 \pm 0.5$	$2.8 \pm 0.2$	$321 \pm 1$	$324 \pm 1$	133
PLA_24h	$0.55 \pm 0.04$	$317 \pm 1$	$5.4 \pm 0.2$	$8.9 \pm 0.5$	$2.1 \pm 0.2$	$310 \pm 1$	$314 \pm 1$	100

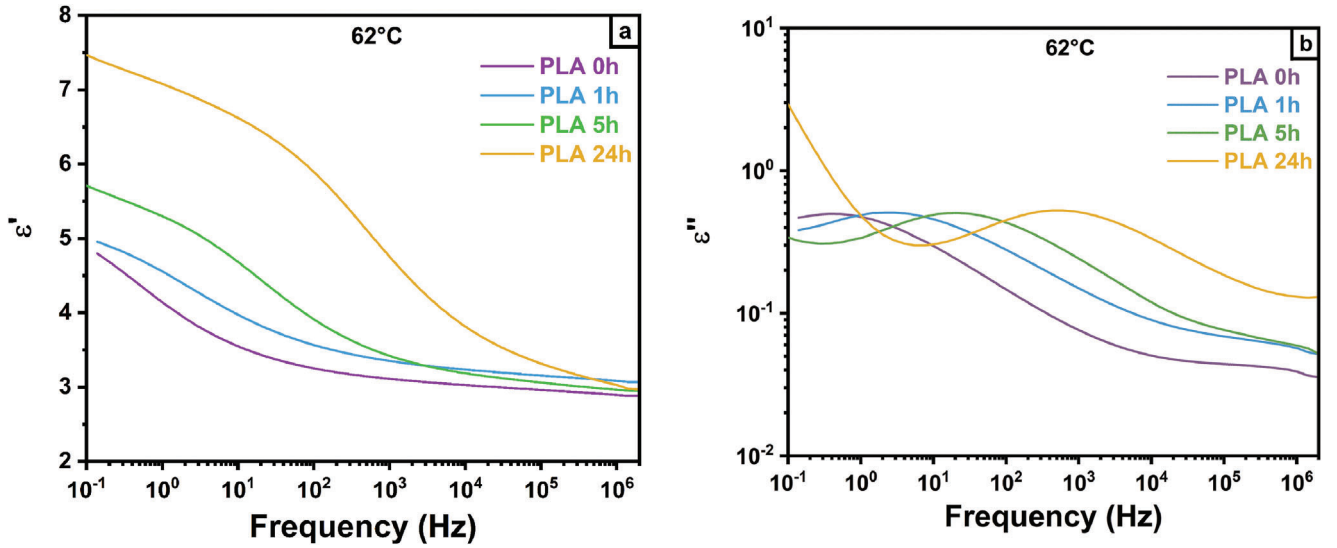


**Figure 6.** a) Real part and b) imaginary part of the permittivity obtained through dielectric relaxation spectroscopy for PLA\_0h, PLA\_1h, PLA\_5h, and PLA\_24h.

## 2.2. Glass Transition Dynamics in PLA Exposed to UV Light

The cooperativity volume  $\xi_{T_\alpha}^3$  has been calculated (Equation (1)) according to the temperature fluctuation approach of the CRR concept as proposed by Donth<sup>[42]</sup>

$$\xi_{T_\alpha}^3 = \frac{\Delta \left( \frac{1}{C_p} \right) k_B T_\alpha^2}{\rho \delta T^2} \quad (1)$$

where  $\delta T$ , estimated from the standard deviation of the  $C''$  Gaussian fit, is the mean temperature fluctuation related to the dynamic glass transition of one CRR,  $k_B$  is the Boltzmann constant,  $\rho$  is the density, and  $C_p$  is the heat capacity at constant pressure. More information regarding the calculation of the CRR size and its structural dependence in PLA can be found in previously published articles.<sup>[6,12,13,43]</sup>

By increasing the UV exposure time up to 24 h,  $\delta T$  increases from 2.6 to 5.4 K and the CRR size  $\xi_{T_\alpha}$  decreases from 3.5 to 2.1 nm. It is worth noting that the CRR calculation is more suited for homogeneous structure, which is hardly certified postdegradation. Nevertheless, the main impact of chain scission on segmental relaxation dynamics is expected to be related to the in-

crease of free volume,<sup>[20]</sup> which is consistent with the decrease of cooperativity when increasing the time of exposure.

Additional information was obtained thanks to DRS measurements. Classically,<sup>[44–46]</sup> the analysis of PLA reveals local motions, as well as a normal mode and a segmental relaxation, the latter being investigated here. In **Figure 6**, presented are the real part  $\epsilon'$  (Figure 6a) and the imaginary part  $\epsilon''$  (Figure 6b) of the complex permittivity  $\epsilon^*$  as a function of frequency during isothermal measurements at  $T = 62^\circ \text{C}$ . The segmental relaxation signature appears sigmoidal in  $\epsilon'$  signal and is characterized by a peak in  $\epsilon''$  signal. Its location is consistent with previous observations.<sup>[45,46]</sup> It is shifted with the UV exposure, as could be anticipated from MT-DSC results. In comparison with PLA\_0h, the transition is indeed recorded at higher frequencies, i.e., at lower relaxation times, in UV-exposed PLAs, which is a characteristic of higher-mobility systems. This is the consequence of the average molecular weight reducing.<sup>[45]</sup>

The temperature dependence of the relaxation time  $\tau$  obtained from DRS investigations is plotted in **Figure 7**. MT-DSC data have been added, for which measurements were performed with an oscillation period of 60 s corresponding to a solicitation frequency about 0.017 Hz, providing  $T_{\alpha \text{ MT-DSC}}$  at a given relaxation time  $\tau$  equal to  $\approx 10 \text{ s}$ . We observe that  $T_{\alpha \text{ MT-DSC}}$  and



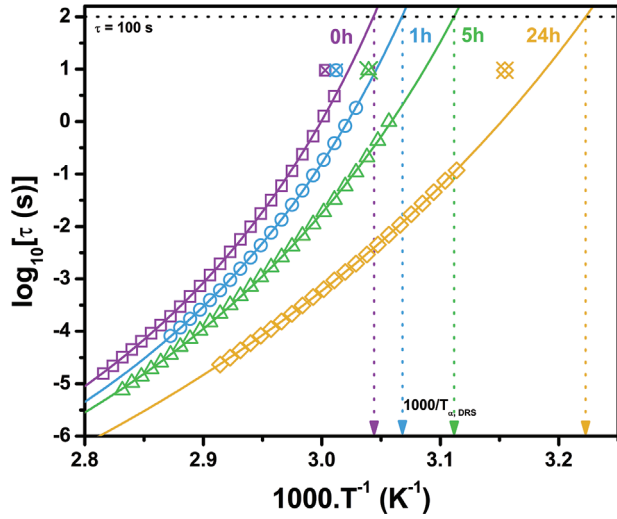


**Figure 7.** Relaxation time versus inverse temperature, depicting the segmental relaxation for PLA\_0h, PLA\_1h, PLA\_5h, and PLA\_24h. Solid curves correspond to the VFTH fitting given in Equation (3). Dotted arrows highlight the segmental relaxation temperature at a relaxation time of 100 s. Crossed symbols indicate the glass transition temperature at midpoint obtained from MT-DSC.

$T_{\alpha\text{DRS}}(\tau = 10 \text{ s})$  vary similarly with the time of exposure, and their values are roughly consistent by considering that the uncertainty regarding  $T_{\alpha}$  increases with  $\delta T$ .<sup>[12]</sup> Furthermore, one can observe that the increase of the relaxation time, by approaching the glass transition  $T_g$ , is less and less brutal with the increasing UV exposure time (here  $T_g$  is arbitrarily defined as the temperature for which the relaxation time  $\tau = 100 \text{ s}$ , leading to  $T_g = T_{\alpha\text{DRS}}(\tau = 100 \text{ s})$ ). The fragility index  $m$  introduced by Angell<sup>[18]</sup> allows classifying glass-forming liquids by their degree of deviation from Arrhenius behavior at  $T_g$  (Equation (2))

$$m = \left. \frac{d \log_{10}(\tau)}{d \left( \frac{T}{T_g} \right)} \right|_{T=T_g} \quad (2)$$

In the classification of Angell, the systems for which  $m$  approaches 16 are “strong.” On the other hand, high values of  $m$  are characteristic of “fragile” liquid glass formers, for which the degree of deviation from Arrhenius behavior is high, which is generally the case for polymers. In that case, the relaxation time versus inverse temperature curve can be fitted by a Vogel–Fulcher–Tammann–Hesse (VFTH) law (Equation (3))

$$\tau = \tau_0 \exp \left( \frac{DT_V}{T - T_V} \right) \quad (3)$$

in which  $D$  is a dimensionless parameter related to the slope variation (steepness strength),  $\tau_0$  is a pre-exponential factor, and  $T_V$  is the Vogel temperature. For PLA\_0h,  $m$  is close to 150 in consistence with values previously reported.<sup>[13]</sup> With the increase of the exposure time up to 24 h,  $m$  decreases down to 100 (Table 3), which is consistent with the decrease of the molecular weight.<sup>[44]</sup> It is worth mentioning that, in comparison with previous stud-

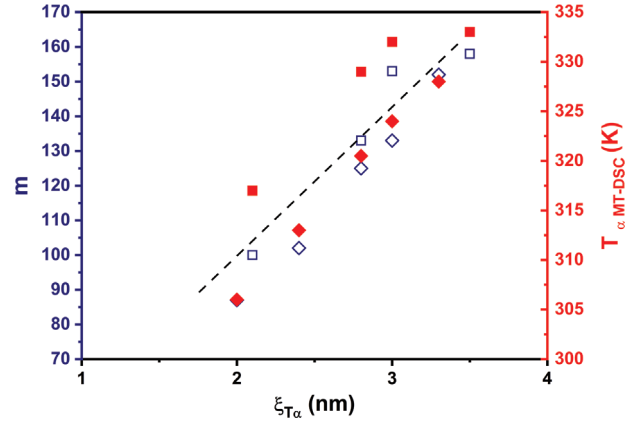


**Figure 8.** Fragility index (empty symbols) and dynamic glass transition temperature (filled symbols) from MT-DSC versus the CRR size. Squared symbols are related to UV-exposed PLA (present study) and diamond symbols correspond to plasticized PLA.<sup>[12]</sup>

ies by other authors,<sup>[21]</sup> the decrease of the kinetic fragility that we report is more pronounced. This is probably caused by the decrease of the molecular weight being stronger in this study, as the degradation conditions have been selected to be severe. In **Figure 8**,  $m$  and  $T_{\alpha\text{MT-DSC}}$  are plotted as a function of  $\xi_{Ta}$ , showing a clear correlation between the relaxation parameters. Previously published data<sup>[12]</sup> regarding plasticized PLA have been added. A linear trend is clearly visible, on which all systems align. According to literature,<sup>[13–15]</sup> this correlation is not systematic. Thus, it is interesting to observe that the effect of UV exposure on the segmental dynamics looks similar to the one generated by the plasticization of PLA. For example, PLA\_24h exhibits similar  $m$  than PLA being plasticized by about 10% acetyltributylcitrate (ATBC). Plasticization does not induce any significant change of molecular weight, but causes the breaking of interchain interactions, leading to an increase of free volume. The control of the degradation of PLA has known recent achievements regarding enzymatic reactions that show that chemical aging is a topic of primary concern.<sup>[47]</sup> Therefore, further investigations regarding the free volume variations in UV-exposed PLAs will certainly be of interest.

### 3. Conclusion

Depicting degradation under UV exposure is challenging because degradation is the result of several chemical reactions, often simultaneous, differently impacting the chemical structure. In this study, we observe that the CRR concept helps following the degradation advancement of PLA. The cooperativity seems to straightforwardly decrease with UV exposure independently on the degradation reactions, although different mechanisms were evidenced. To explain this result, it is assumed that these degradation reactions share a similar disruptive effect, increasing the free volume. Moreover, the variations of both fragility and calorimetric glass transition, two essential features of segmental relaxation, have been efficiently described using the CRR concept. For these reasons, the study of relaxation dynamics emerges as an interesting complement to structural characterization techniques in order to follow the degradation processes.

## 4. Experimental Section

**Materials:** PLA 4042D (4.3% D-lactic acid and 95.7% L-lactic acid) pellets were provided by Natureworks, with number average  $M_n$  and weight average  $M_w$  molecular weights being equal to 116 and 188 kg mol<sup>-1</sup>, respectively. Pellets were dried in an oven for 24 h at 50 °C prior to thermomolding to prevent hydrolytic degradation. Drying in the glass transition range instead of the rubbery state was an attempt to minimize, as much as possible, the risks of initiating thermo-oxidation. The pellets were then thermomolded between two hot plates for 2 min at 180 °C under 10 bar pressure. The obtained films of about 200 μm thickness were directly quenched into water in order to obtain fully amorphous PLA films. The amorphous character of the samples was then controlled by DSC.

**UV Irradiation:** PLA films were placed 10 cm under a metal halide Dymax 5000 polychromatic lamp. The power bulb was set to 400 W. The maximum measured intensity at the wavelength of 365 nm was 375 W cm<sup>-2</sup>. The lamp was turned on 10 min prior to UV exposure to ensure full intensity and repeatability. A dry nitrogen gas flow (99.99% purity, Air Liquide) was injected into the curing box throughout the whole exposure to decrease the content of oxygen possibly interacting with PLA. The UV exposure time were set to 1, 5, 20, and 24 h, respectively. Samples were named accordingly PLA\_0h (no exposure), PLA\_1h, PLA\_5h, PLA\_20h, and PLA\_24h.

**Material Characterization:** FT-IR measurements were performed in attenuated total reflectance (ATR) mode using a diamond crystal plate accessory on PLA films with the help of the Nicolet iS10 FT-IR spectrometer from Thermoscientific, equipped with a helium–neon laser source, a Ge/KBr beam splitter, and a deuterated triglycine sulfate (DTGS) pyroelectric detector. The spectra were collected in the 4000–400 cm<sup>-1</sup> wavenumber range. The acquisition parameters were chosen as follows: 16 scans and 4 cm<sup>-1</sup> medium resolution. The characteristic vibration bands of neat and UV-exposed PLAs were attributed with the help of the OMNIC series acquisition software.

Samples were analyzed using a GPC system comprising a Waters HPLC apparatus (Waters 717+ apparatus) with a Styragel SE5 column, and with a THF flow rate equal to 1 mL min<sup>-1</sup>. Detection was performed using a Waters 2414 Refractive Index ( $T_{\text{detector}} = 40$  °C). GPC column was calibrated with PS standards (Shodex).

MT-TGA experiments were performed under a 25 mL min<sup>-1</sup> nitrogen flow, with a balance purge of nitrogen at 25 mL min<sup>-1</sup>, in a Thermal Analysis Discovery apparatus. A sample of about 5 mg mass was put in platinum pans compatible with high temperature. The calibration procedure included a baseline with empty furnace, the calibration in temperature by referring to the Curie point of nickel, and the calibration in mass and mass loss using temperature-resistant standards, and calcium oxalate respectively. The analyses were carried out from 30 to 700 °C with modulation parameters, i.e., amplitude = 5 K, period = 200 s, and heating rate = 5 K min<sup>-1</sup>, being chosen to provide a minimum of five cycles within the degradation process range. The MT-TGA procedure was based on the idea of Flynn,<sup>[48]</sup> to derive kinetic data from thermogravimetric measurements.<sup>[49]</sup> The oscillatory temperature equation for thermogravimetry:  $dw/dt = CdT/dt + f(t, T)$  is analogous to MT-DSC one:  $dQ/dt = Cp dT/dt + f(t, T)$ , with the exception that in MT-TGA the heating rate-dependent term  $CdT/dt$  is equal to zero.<sup>[50]</sup> Therefore,  $dw/dt$ , the rate of mass loss, is directly proportional to  $f(t, T)$ , the kinetic term, which engulfs the relationship between the rate of reaction and the amount of material, as well as the Arrhenius temperature dependence.<sup>[50]</sup> In MT-TGA, one uses  $d\alpha_p/d\alpha_v$ , the ratio for adjacent peaks, and valleys, of the periodic rate of reaction, to evaluate  $f(t, T)$ , which leads to Equation (4) for the activation energy  $E_a$

$$E_a = \frac{R(T^2 - A^2) \ln \frac{d\alpha_p}{d\alpha_v}}{2A} \quad (4)$$

where  $T$  is the average value of oscillatory temperature and  $A$  is the amplitude of the temperature oscillation. This equation allows estimating  $E_a$  from the perturbations in the derivative caused by the temperature modulation without any preconception regarding the kinetic model.<sup>[51]</sup>

MT-DSC experiments were performed on a DSC Q2000 Thermal Analysis instrument. The samples were encapsulated in Tzero DSC aluminum alloy pans with an average weight of 6–7 mg. The pan was positioned in the furnace with the aim of ensuring a good surface contact with the thermal sensor. Calibration in temperature was carried out using standards of indium and benzophenone. Calibration in energy was carried out using standard values of indium. The specific heat capacity for each sample was measured using sapphire as a reference. The modulation parameters were an oscillation amplitude of 0.318 K, an oscillation period of 60 s, and a heating rate of 2 K min<sup>-1</sup>. During experiment, the furnace was permanently swept by a nitrogen flow (50 mL min<sup>-1</sup>). The signals needed for the CRR size calculation, i.e., the in-phase  $C'$  and the out-of-phase  $C''$  components of the complex heat capacity  $C^*$ , were obtained by applying the complete deconvolution procedure proposed by Reading and co-workers.<sup>[52]</sup> Phase corrections were performed as suggested by Weyer et al.<sup>[53]</sup>

Dielectric relaxation spectra were measured with an Alpha Analyzer from Novocontrol with a frequency range of 10<sup>-1</sup>–10<sup>6</sup> Hz. The measurements were performed using parallel electrodes (upper electrode diameter = 30 mm, sample thickness = 200 μm) regarding PLA\_0h and PLA\_1h. For these two samples, the UV exposure had no impact on the film thickness, neither the homogeneity of the sample. However, the outcome was different for long exposure times which completely modified the film shape. Thus, PLA\_5h, and PLA\_24h were melted on interdigitated electrodes. In that specific case, amorphous samples were obtained by putting the interdigitated electrodes in contact with a cold surface stored at -15 °C. The interdigitated electrodes (Novocontrol Technologies DRS1410-20-150 with an effective diameter of 20 mm, loss factor accuracy  $\tan \delta = 0.001$ ) were calibrated according to the Novocontrol requirement, i.e., by defining empty cell capacity  $C_0$  and substrate capacity  $C_{su}$  using a standard material (mineral B-oil, Vacuubrand). The measurements were then performed from 10 below to 25 °C above the MT-DSC glass transition temperature, with a temperature step of 1 K during the segmental relaxation observation. The temperature was controlled through a heated nitrogen flow gas using a Quatro Cryosystem. The segmental relaxation was analyzed by fitting the complex permittivity  $\epsilon^*$  at each recorded temperature with the Havriliak–Negami (HN) complex function.

## Conflict of Interest

The authors declare no conflict of interest.

## Data Availability Statement

The data that support the findings of this study are available from the corresponding author upon reasonable request.

## Keywords

chromatography, glass transition, infrared, polylactide, UV degradation

Received: March 11, 2022

Revised: May 5, 2022

Published online: July 7, 2022

- [1] V. Ducruet, S. Domenek, in *Biodegradable and Bio-Based Polymers: Environmental and Biomedical Applications* (Eds: S. Kalia, L. Averous) Scrivener Publishing LLC, Beverly, MA 2015, pp. 171–224.
- [2] U. Sonchaeng, F. Iñiguez-Franco, R. Auras, S. Selke, M. Rubino, L.-T. Lim, *Prog. Polym. Sci.* **2018**, *86*, 85.
- [3] G. Kfoury, J.-M. Raquez, F. Hassouna, J. Odent, V. Toniazio, D. Ruch, P. Dubois, *Front. Chem.* **2013**, *1*, 32.



- [4] M. Wang, Y. Wu, Y.-D. Li, J.-B. Zeng, *Polym. Rev.* **2017**, *57*, 557.
- [5] A. Bouzouita, D. Notta-Cuvier, J.-M. Raquez, F. Lauro, P. Dubois, in *Advances in Polymer Science: Industrial Applications of Poly(Lactic Acid)* (Eds: M. L. Di Lorenzo, R. Androsch), Vol. 282, Springer, Cham, Switzerland **2017**, pp. 177–219.
- [6] S. Araujo, N. Delpouve, S. Domenek, A. Guinault, R. Golovchak, R. Szatanik, A. Ingram, C. Fauchard, L. Delbreilh, E. Dargent, *Macromolecules* **2019**, *52*, 6107.
- [7] G. Adam, J. H. Gibbs, *J. Chem. Phys.* **1965**, *43*, 139.
- [8] A. Dhotel, Z. Chen, J. Sun, B. Youssef, J.-M. Saiter, A. Schönhals, L. Tan, L. Delbreilh, *Soft Matter* **2015**, *11*, 719.
- [9] C. V. Grigoras, A. G. Grigoras, *J. Therm. Anal. Calorim.* **2011**, *103*, 661.
- [10] M. Nakanishi, R. Nozaki, *Phys. Rev. E* **2011**, *84*, 011503.
- [11] T. Sasaki, T. Uchida, K. Sakurai, *J. Polym. Sci., Part B: Polym. Phys.* **2006**, *44*, 1958.
- [12] S. Araujo, N. Delpouve, A. Dhotel, S. Domenek, A. Guinault, L. Delbreilh, E. Dargent, *ACS Omega* **2018**, *3*, 17092.
- [13] N. Delpouve, L. Delbreilh, G. Stoclet, A. Saiter, E. Dargent, *Macromolecules* **2014**, *47*, 5186.
- [14] M. Sharma, G. Madras, S. Bose, *Macromolecules* **2015**, *48*, 2740.
- [15] L. Hong, V. N. Novikov, A. P. Sokolov, *J. Non-Cryst. Solids* **2011**, *357*, 351.
- [16] S. Araujo, F. Batteux, W. Li, L. Butterfield, N. Delpouve, A. Esposito, L. Tan, J.-M. Saiter, M. Negahban, *J. Polym. Sci., Part B: Polym. Phys.* **2018**, *56*, 1393.
- [17] J. A. S. Puente, B. Rijal, L. Delbreilh, K. Fatyeyeva, A. Saiter, E. Dargent, *Polymer* **2015**, *76*, 213.
- [18] C. A. Angell, *J. Non-Cryst. Solids* **1985**, *73*, 1.
- [19] K. Kunal, C. G. Robertson, S. Pawlus, S. F. Hahn, A. P. Sokolov, *Macromolecules* **2008**, *41*, 7232.
- [20] J. D. Badia, E. Strömberg, S. Karlsson, A. Ribes-Greus, *Polym. Degrad. Stab.* **2012**, *97*, 670.
- [21] J. D. Badia, L. Monreal, V. Sáenz De Juano-Arbona, A. Ribes-Greus, *Polym. Degrad. Stab.* **2014**, *107*, 21.
- [22] G. Kister, G. Cassanas, M. Vert, *Polymer* **1998**, *39*, 267.
- [23] D. Rasselet, A. Ruellan, A. Guinault, G. Miquelard-Garnier, C. Sologoub, B. Fayolle, *Eur. Polym. J.* **2014**, *50*, 109.
- [24] M. Gardette, S. Thérias, J.-L. Gardette, M. Murariu, P. Dubois, *Polym. Degrad. Stab.* **2011**, *96*, 616.
- [25] E. Ikada, *J. Photopolym. Sci. Technol.* **1997**, *10*, 265.
- [26] S. Belbachir, F. Zairi, G. Ayoub, U. Maschke, M. Naït-Abdelaziz, J. M. Gloaguen, M. Benguediab, J. M. Lefebvre, *J. Mech. Phys. Solids* **2010**, *58*, 241.
- [27] E. Olewnik-Kruszkowska, I. Koter, J. Skopińska-Wisniewska, J. Richert, *J. Photochem. Photobiol., A* **2015**, *311*, 144.
- [28] A. Babanalbandi, D. J. T. Hill, J. H. O'donnell, P. J. Pomery, A. Whitaker, *Polym. Degrad. Stab.* **1995**, *50*, 297.
- [29] A. Copinet, C. Bertrand, S. Govindin, V. Coma, Y. Couturier, *Chemosphere* **2004**, *55*, 763.
- [30] M. Füllbrandt, P. J. Purohit, A. Schönhals, *Macromolecules* **2013**, *46*, 4626.
- [31] Z. Terzopoulou, P. A. Klonos, A. Kyritsis, A. Tziolas, A. Avgeropoulos, G. Z. Papageorgiou, D. N. Bikiaris, *Polymer* **2019**, *166*, 1.
- [32] P. A. Klonos, N. D. Bikiaris, E. Christodoulou, A. Zamboulis, G. Z. Papageorgiou, A. Kyritsis, *Polymer* **2022**, *242*, 124603.
- [33] Z. Grubisic, P. Rempp, H. Benoit, *J. Polym. Sci., Part B: Polym. Lett.* **1967**, *5*, 753.
- [34] P. Dubois, C. Jacobs, R. Jerome, P. Teyssie, *Macromolecules* **1991**, *24*, 2266.
- [35] O. Saito, *J. Phys. Soc. Jpn.* **1958**, *13*, 198.
- [36] R. R. Keuleers, J. F. Janssens, H. O. Desseyn, *Thermochim. Acta* **2002**, *385*, 127.
- [37] K. Cheng, W. T. Winter, A. J. Stipanovic, *Polym. Degrad. Stab.* **2012**, *97*, 1606.
- [38] C. A. Gracia-Fernández, S. Gómez-Barreiro, S. Ruíz-Salvador, R. Blaine, *Prog. Org. Coat.* **2005**, *54*, 332.
- [39] I. C. McNeill, H. A. Leiper, *Polym. Degrad. Stab.* **1985**, *11*, 309.
- [40] F. Signori, M.-B. Coltelli, S. Bronco, *Polym. Degrad. Stab.* **2009**, *94*, 74.
- [41] T. Beslikas, I. Gigos, V. Goulios, J. Christoforides, G. Z. Papageorgiou, D. N. Bikiaris, *Int. J. Mol. Sci.* **2011**, *12*, 6597.
- [42] E. Donth, *J. Non-Cryst. Solids* **1982**, *53*, 325.
- [43] N. Varol, N. Delpouve, S. Araujo, S. Domenek, A. Guinault, R. Golovchak, A. Ingram, L. Delbreilh, E. Dargent, *Polymer* **2020**, *194*, 122373.
- [44] S. M. Moghaddam, B. Quelennec, N. Delpouve, B. Atawa, L. Delbreilh, A. Saiter-Fourcin, E. Passaglia, S. Fiori, *J. Polym. Sci.* **2021**, *59*, 1571.
- [45] J. Ren, O. Urakawa, K. Adachi, *Macromolecules* **2003**, *36*, 210.
- [46] M. Pluta, J. K. Jeszka, G. Boiteux, *Eur. Polym. J.* **2007**, *43*, 2819.
- [47] C. Delre, Y. Jiang, P. Kang, J. Kwon, A. Hall, I. Jayapurna, Z. Ruan, L. Ma, K. Zolkin, T. Li, C. D. Scown, R. O. Ritchie, T. P. Russell, T. Xu, *Nature* **2021**, *592*, 558.
- [48] J. H. Flynn, in *Thermal Analysis* (Eds: R. F. Schwenker, P. D. Garn), Vol. 2, Academic Press, NewYork, NY **1969**, pp. 1111–1126.
- [49] J. E. K. Schawe, *Thermochim. Acta* **2014**, *593*, 65.
- [50] R. L. Blaine, B. K. Hahn, *J. Therm. Anal.* **1998**, *54*, 695.
- [51] V. Mamleev, S. Bourbigot, *Chem. Eng. Sci.* **2005**, *60*, 747.
- [52] A. A. Lacey, D. M. Price, M. Reading, in *Modulated Temperature Differential Scanning Calorimetry* (Eds: M. Reading, D. J. Hourston), Vol. 6, Springer, Dordrecht, Netherlands **2006**, pp. 1–81.
- [53] S. Weyer, A. Hensel, C. Schick, *Thermochim. Acta* **1997**, *267*, 304.